# Penning ionization of HCHO, CH2CH2, and CH2CHCHO by collision with He*(23S) metastable atoms

**ARTICLE** *in* THE JOURNAL OF PHYSICAL CHEMISTRY · SEPTEMBER 1995

Impact Factor: 2.78 · DOI: 10.1021/j100039a010



**6 AUTHORS**, INCLUDING:

Hideo Yamakado
Wakayama University
**40** PUBLICATIONS **647** CITATIONS

SEE PROFILE

Tomohide Takami
Kogakuin University
**74** PUBLICATIONS **1,339** CITATIONS

SEE PROFILE

# Penning Ionization of HCHO, $CH_2CH_2$, and $CH_2CHCHO$ by Collision with He*($2^3S$) Metastable Atoms

**Koichi Ohno,* Kohji Okamura, Hideo Yamakado, Shigeo Hoshino, Tomohide Takami,† and Masayo Yamauchi**

*Department of Chemistry, Faculty of Science, Tohoku University, Aramaki, Aoba-ku, Sendai 980, Japan*

*Received: February 3, 1995; In Final Form: April 3, 1995⊗*

Penning ionization of formaldehyde (HCHO), ethylene ($CH_2CH_2$), and acrolein ($CH_2CHCHO$) upon collision with metastable He*($2^3S$) atoms was studied by collision-energy-resolved Penning ionization electron spectroscopy. Collision energy dependence of Penning ionization cross sections (CEDPICS) indicates that interaction potentials are highly anisotropic between He*($2^3S$) atoms and the planar molecules investigated. Attractive interactions around the oxygen atom of the C=O group in the aldehydes were found to be stronger in the molecular plane than out-of-plane. In the case of ethylene, local interaction potentials with He* atoms were characterized more precisely. The regions of $\pi$ electrons undergo attractive interactions, whereas intraplane potentials are highly repulsive; the intraplane direction to the middle of the methylene unit gives a softer repulsion than the collinear direction to the H atom in the CH bond.

## I. Introduction

The anisotropic and specific nature of molecular interactions can be characterized by observing collision processes of molecules with atomic probes. In a chemi-ionization process known as Penning ionization,[1−4] a molecule M collides with a metastable atom A* having an excitation energy larger than the lowest ionization potential(IP) of the molecule. Kinetic energy of the ejected electron $e^-$ in the ionization process depends on the produced ionic state of the molecule $M_i^+$;

$$A^* + M \rightarrow A + M_i^+ + e^- \quad (1)$$

The measurement for the total ion intensity will give the total ionization cross sections, and the measurements for the energy-resolved electron intensities will provide the partial ionization cross sections.

One of the important variables in the collision process is the relative collision energy $E$, because the cross sections may either increase or decrease with an increase of the collision energy depending upon interactions involved.[2] Total ionization cross sections for various atoms and molecules in collision with metastable atoms have been studied previously.[5−12] The collision energy dependence of the total ionization cross sections has been measured as a function of the collision energy controlled by means of a velocity selector for the metastable atoms. It has been observed that the ionization cross section decreases with the increase of $E$ for the collision of a Hg atom with He*,[2,5,9] indicating that the interaction potential between He* and Hg atoms is attractive. On the other hand, the ionization cross section increases with an increase of $E$ for an Ar atom with He*,[5−9] and the interaction potential is repulsive.

In the case of a target molecule, the interaction potential is highly anisotropic. It is, however, difficult to obtain information on the anisotropy of the interaction potential from the study of the total ionization cross section, since the total cross section reflects only an average potential; when several ionic states can be produced by ionization of a target molecule in collision with a metastable atom, the total ionization cross section would then be the sum of the partial ionization cross sections (ionization cross sections for different ionic states).

A given partial ionization cross section for a closed shell molecule can be ascribed to the ionization of a given molecular orbital (MO) of the target molecule. It has been shown from the study of partial ionization cross sections or branching ratios for Penning ionization that the most effective geometrical situations for the collisional ionization are different depending upon the electron distribution of the target molecular orbitals.[13,14] Since molecular orbitals are highly anisotropic with electron densities more or less localized on a certain part of the molecule, the collision energy dependence of partial ionization cross sections will not be the same, reflecting the anisotropy of the interaction potential. The anisotropy of the interaction potential can then be deduced from the collision energy dependence of partial ionization cross sections.

In Penning ionization electron spectroscopy (PIES), the kinetic energies of electrons ejected from target MOs on Penning ionization are analyzed.[15] Since selection of ionic states can be made by the choice of electron kinetic energies to be analyzed, the collision energy dependence of the energy-analyzed electron intensity yields the collision energy dependence of the partial Penning ionization cross sections. In our recent studies,[16−20] a combination of time-of-flight (TOF) selections of metastable atom velocities with electron kinetic energy analyses has been used to develop two types of novel techniques; (1) measurements of the collision energy dependence of Penning ionization cross sections (CEDPICS) for a particular ionic state of the target molecule $M_i^+$, $\sigma_i(E)$, and (2) measurements of collision-energy-resolved Penning ionization electron spectra (CERPIES). CERPIES have also been measured by a different method utilizing velocity-controlled supersonic metastable beams.[4,21,22]

By means of the above techniques, we found repulsive interaction potentials for He*($2^3S$) + $N_2$ and He*($2^3S$) + $CO_2$, and repulsive walls for end-on collisions were shown to be harder than those for side-on collisions.[17] Interaction potentials between saturated and unsaturated hydrocarbons were found to

† Present address: Department of Physics, Graduate School of Science, The University of Tokyo, Japan.

⊗ Abstract published in *Advance ACS Abstracts,* September 1, 1995.

0022-3654/95/2099-14247$09.00/0 

be repulsive except for the $\pi$ orbital region, where the interaction potential with metastable atoms was shown to be attractive.[18,19] The study of $CH_3SCN$, $CH_3NCO$, and $CH_3NCS$ indicated that the interaction potential was repulsive around the methyl group and attractive around the pseudohalide group.[20]

In the present paper, we investigate the interaction potential between the He*($2^3S$) atom and the HCHO, $CH_2CH_2$, or $CH_2$-CHCHO molecule; acrolein ($CH_2CHCHO$) is a composite system of a couple of planar isoelectronic molecules, ethylene ($CH_2CH_2$) and formaldehyde (HCHO).

## II. Experiment

The experimental apparatus used in the present study has been reported previously.[16-18] The kinetic energy of electrons ejected by collisional ionization or photoionization was determined by a hemispherical electrostatic deflection type analyzer at a collection angle of 90°[23] with respect to the incident He* or photon beam. The energy resolution of the electron energy analyzer was estimated to be 40 meV from the full width at half-maximum (fwhm) of the $Ar^+(^2P_{3/2})$ peak in the He I ultraviolet photoelectron spectrum (UPS). Ultraviolet photoelectron spectra were measured by using the He I resonance photons (21.22 eV) produced by a dc discharge in pure helium gas. The transmission of the electron energy analyzer was determined by comparing our UPS data with those by Gardner and Samson[24] and Kimura et al.[25]

A nozzle discharge source with a tantalum hollow cathode was used to produce metastable He*($2^3S$ 19.82 eV, $2^1S$ 20.62 eV) beams.[18] A water-cooled helium dc lamp was used to eliminate He*($2^1S$) components from the metastable atom beams. The He* beam was pulsed with a mechanical chopper rotating at 400 Hz and introduced into a reaction chamber at 504 mm downstream from the chopper. The TOF spectrum of He*($2^3S$) atoms $I_{He^*}(V_{He^*})$ was obtained by detecting time-dependent signals of electrons emitted from a stainless steel plate inserted at the center of the reaction chamber.[17] TOFs of secondary electrons from the metal surface to the detector are negligibly short in comparison with TOFs of the He* atoms. The efficiency of the secondary electron from a metal plate was considered to be constant in the observed collision energy range.[17]

In the mode of CERPIES measurements, two spectra with a low collision energy of ca. 95 meV on average (75−115 meV) and a high collision energy of ca. 210 meV (170−360 meV) were recorded at a lowered electron energy resolution of 250 meV (fwhm for He I UPS of Ar) in order to obtain higher counting rates of electrons.[19]

To determine the collision energy dependence of Penning ionization cross section (CEDPICS) for a given ionic state, the time-dependent spectrum of respective Penning electrons $I_e$ was measured by the energy fixed mode of the electron energy analyzer (fwhm for He I UPS of Ar was 250 meV). Since the time-resolved spectrum gives the electron intensity $I_e$ as a function of the He* velocity $V_{He^*}$, the collision energy dependence of the partial ionization cross section $\sigma_i(E)$ can be determined by the following equation:

$$\sigma_i(V_r) = c[I_e(V_{He^*})/I_{He^*}(V_{He^*})](V_{He^*}/V_r) \quad (2)$$

where $c$ is a constant and

$$V_r = [V_{He^*}{}^2 + (3kT/M)]^{1/2} \quad (3)$$

where $k$ is the Boltzmann constant, and $T$ and $M$ are the gas temperature and the mass of the target molecule, respectively. Finally, $\sigma_i(V_r)$ is converted to $\sigma_i(E)$ by the equation

$$E = (1/2)\mu V_r^2 \quad (4)$$

where $\mu$ is the reduced mass of the system.

## III. Calculations

To discuss observed CEDPICS, interaction potential curves with the metastable atom approaching the target molecule along several directions were calculated using the *ab initio* molecular orbital method.[26] Difficulties usually associated with *ab initio* calculations for excited states embedded in an ionization continuum were avoided by the following treatment based on the well-known resemblance between He*($2^3S$) and Li($2^2S$). It has been shown[27] that the shape of the velocity dependence of the total scattering cross section of He*($2^3S$) by He, Ar, and Kr is very similar to that of Li($2^2S$). The location of the interaction potential well and its depth have also been found to be very similar for interactions of He*($2^3S$) and Li($2^2S$) with various target systems.[2,5,28,29] Due to these findings, a Li($2^2S$) atom was used in place of a He*($2^3S$) atom for potential curve calculations. The geometries of target molecules were fixed at experimental neutral ground-state structures. The *ab initio* MO calculations were performed at the level of the unrestricted Hartree−Fock (UHF) scheme utilizing the Gaussian-92 program package.[30] The 4-31G basis sets were employed with the standard diffuse functions (H, C, O) and the standard polarization functions (H, C, O).[26] This choice of basis functions has been found to be satisfactory for the purpose of our studies.[31] Electron correlation effects were taken into account using second-order Møller−Plesset perturbation theory (MP2).

Contour maps of the position of the Li atom for given potential energies (isopotential energy maps) were drawn for HCHO with the aid of a simple spline program on a personal computer. To obtain potential energy contour maps for vertical and horizontal planes of HCHO, 163 points of single-point *ab initio* MO calculations were performed.

Schematic representation of MOs with circles and ellipses were used as in a previous study.[32] In-plane p type orbitals were shown by pairs of ellipses. The out-of-plane component of p orbitals was shown by a dashed circle. Valence s orbitals were shown by solid circles. Signs of orbital coefficients were indicated by the thickness of the curves. Electron density contour maps were also used as in previous studies.[13,14] Thick solid curves in electron density maps indicate the repulsive molecular surface approximated by atomic spheres of van der Waals radii.[33] Electron density contour maps for $\sigma$ orbitals were shown in the molecular plane, and those for $\pi$ orbitals were shown in a vertical plane including the respective double bond.

## IV. Results

Figures 1−3 show observed CEDPICS for HCHO, $CH_2CH_2$, and $CH_2CHCHO$, respectively. Partial Penning ionization cross sections $\sigma$ and collision energy $E$ are plotted as $\log \sigma - \log E$ curves. The cross sections are shown in arbitrary units. The calculated electron density maps of the molecular orbitals corresponding to the observed ionic states are also shown together with the simplified molecular orbital diagrams.

Table 1 lists the vertical ionization potential (determined from the He I UPS) and the assignments of the observed bands. The He I UPS for HCHO and $CH_2CH_2$ were essentially the same as the earlier data.[25,32] The conventional PIES without velocity selection for HCHO[32] and $CH_2CH_2$[34] were also the same as those reported previously. Figure 4 shows the UPS and PIES for $CH_2$-CHCHO. The spectra in Figure 4 contain impurity bands due to $H_2O$, as specified by arrows. Figures 5 and 6 show observed

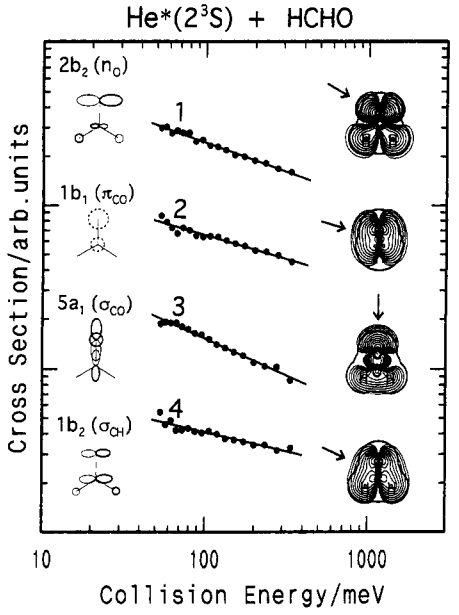


**Figure 1.** Collision energy dependences of Penning ionization cross sections for HCHO with He*($2^3$S).

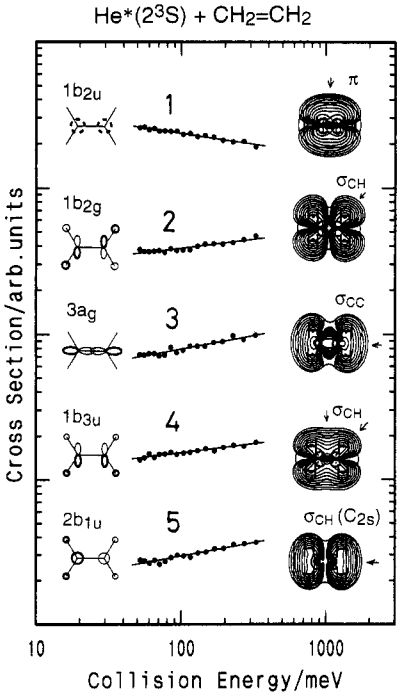


**Figure 2.** Collision energy dependences of Penning ionization cross sections for $CH_2CH_2$ with He*($2^3$S).

CERPIES for HCHO and $CH_2CHCHO$. Hot spectra at the higher collision energy are shown by dashed curves, and cold spectra at the lower collision energy are shown by solid curves. The relative intensity of the two spectra is normalized in the figure using the data of the CEDPICS. CERPIES for $CH_2CH_2$ were nearly the same as the earlier work.[34] The peak energy shifts in PIES measured with respect to the "nominal" energy $E_0$ ($E_0$ = the difference between metastable excitation energy and target ionization potential) are also shown in Table 1. The peak shift of the $\sigma_{CH}(1b_2)$ band in the PIES of HCHO was not determined due to the small relative intensity and strong overlapping with the $\sigma_{CO}$ band. The peak shifts for some other bands were also not listed because of similar reasons. The values of the slope $m$ of the log $\sigma$ − log $E$ plots as well as the calculated $s$ and $d$ parameters (see below) are listed in Table 1. The slope parameters $m$ were estimated in a collision energy

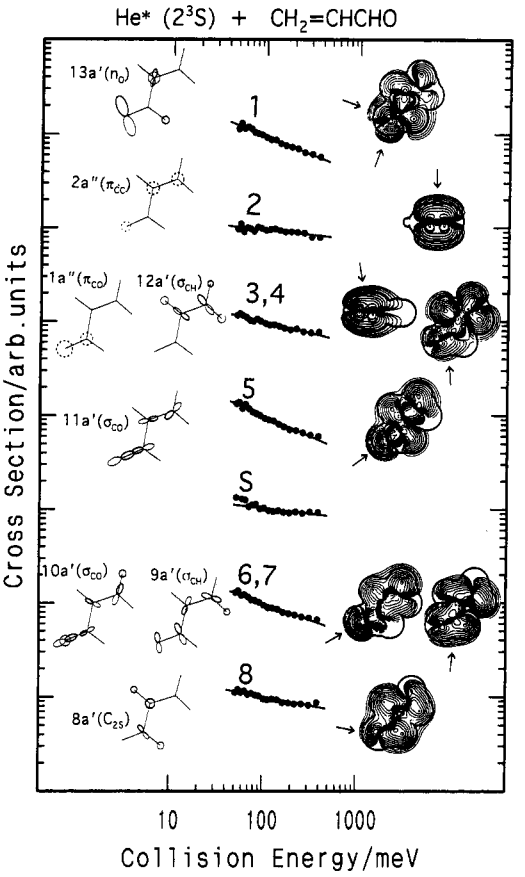


**Figure 3.** Collision energy dependences of Penning ionization cross sections for $CH_2CHCHO$ with He*($2^3$S).

**TABLE 1: Band Assignment, Ionization Potential (IP), Peak Energy Shift (ΔE), and Obtained Parameters (See Text)**

| molecule | band | orbital character | IP/eV | ΔE/eV | m | s | d/(au$^{-1}$) |
|---|---|---|---|---|---|---|---|
| HCHO | 1 | $n_O$ ($2b_2$) | 10.88 | −0.12 | −0.36 ± 0.03 | 5.6 | |
| | 2 | $\pi_{CO}$ ($1b_1$) | 14.50 | −0.07 | −0.29 ± 0.03 | 7.0 | |
| | 3 | $\sigma_{CO}$ ($5a_1$) | 16.00 | −0.12 | −0.44 ± 0.02 | 4.6 | |
| | 4 | $\sigma_{CH}$ ($1b_2$) | 16.60 | | −0.23 ± 0.05 | 8.8 | |
| $CH_2CH_2$ | 1 | $\pi_{CC}$ ($1b_{2u}$) | 10.51 | −0.03 | −0.15 ± 0.02 | 13.3 | |
| | 2 | $\sigma_{CH}$ ($1b_{2g}$) | 12.85 | 0.14 | 0.12 ± 0.02 | | 2.83 |
| | 3 | $\sigma_{CC}$ ($3a_g$) | 14.66 | 0.00 | 0.18 ± 00.02 | | 2.57 |
| | 4 | $\sigma_{CH}$ ($1b_{3u}$) | 15.87 | 0.15 | 0.12 ± 0.02 | | 2.83 |
| | 5 | $C_{2s}$ ($2b_{1u}$) | 19.10 | 0.24 | 0.18 ± 0.02 | | 2.57 |
| $CH_2CHCHO$ | 1 | $n_O$ (13a') | 10.10 | −0.26 | −0.39 ± 0.03 | 5.1 | |
| | 2 | $\pi_{CC}$ (2a") | 10.92 | 0.00 | −0.10 ± 0.03 | 19.8 | |
| | 3, 4 | $\pi_{CO}$ (1a") | 13.7 | −0.17 | −0.23 ± 0.03 | 8.7 | |
| | | $\sigma_{CH}$ (12a') | 13.7 | | | | |
| | 5 | $\sigma_{CO}$ (11a') | 14.6 | −0.36 | −0.43 ± 0.02 | 4.7 | |
| | S | | 15.5 | | −0.11 ± 0.05[a] | 18.3 | |
| | 6, 7 | $\sigma_{CO}$ (10a') | 16.05 | −0.27 | −0.35 ± 0.02 | 5.7 | |
| | | $\sigma_{CH}$ (9a') | 16.35 | | | | |
| | 8 | $C_{2s}$ (8a') | 18.82 | 0.02 | −0.18 ± 0.04 | 11.0 | |

[a] Because of overlapping contributions from nearby bands, the slope parameter value for the band S was estimated between 70 and 400 meV, whereas for other bands the values were estimated between 50 and 400 meV.

range 50−400 meV by a linear least-squares method. The $s$ values were calculated when $m < 0$, and the $d$ values were calculated when $m > 0$. The $d$ values are shown in atomic units (au).

Figure 7 shows isopotential energy contour maps for HCHO; the map for the out-of-plane (a) and that for the molecular plane (b) are shown separately. The depth of the potential well is ca. 340 meV. Figure 8 shows the model interaction potential $V(R)$ for $CH_2CH_2$. The distance $R$ is measured from the center of mass of the molecule when the He* (Li) atom is located in

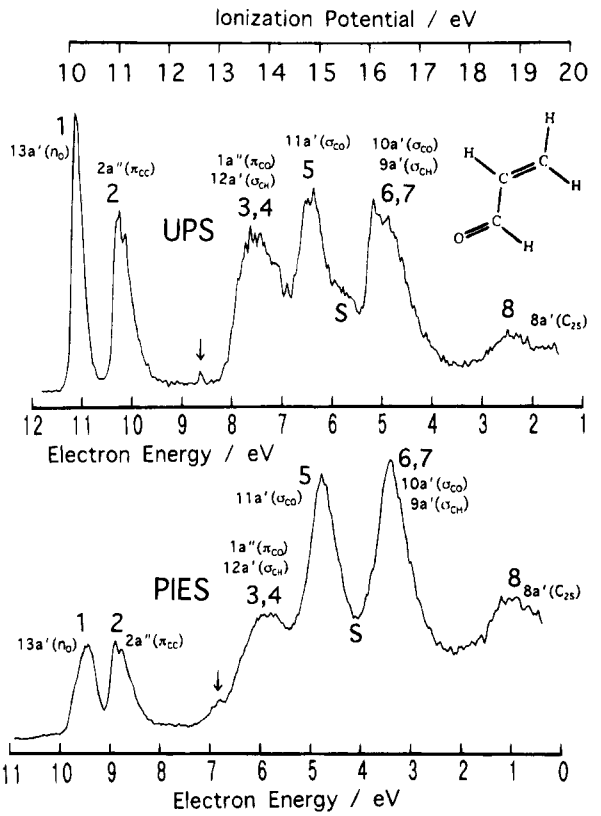


**Figure 4.** He I UPS and He*($2^3$S) PIES for $CH_2CHCHO$.

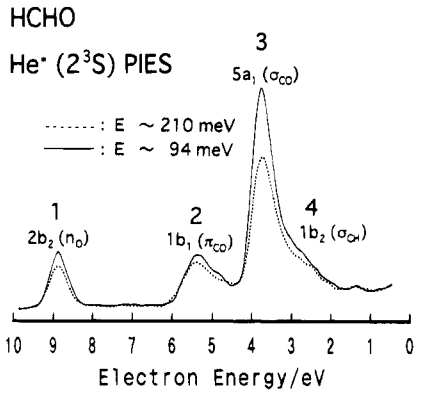


**Figure 5.** Collision-energy-resolved He*($2^3$S) Penning ionization electron spectra of HCHO (dashed curve at 210 meV, solid curve at 94 meV).

a plane bisecting the CC bond, otherwise $R$ is the distance from the nearest C atom. Isopotential contour maps for $CH_2CH_2$ were not obtained because of the limitation of the computation time.

## V. Discussion

**A. Simple Model for CEDPICS and Parameters, *s*, *b*, and *d*.** If the simple theoretical models[2] established for isotropic target systems can be applied effectively for anisotropic systems, parameters listed in Table 1 can be obtained.

For the low collision energy region, attractive interactions are important because the centrifugal barrier becomes low enough to enhance the reaction cross sections.

When the attractive interaction of $R^{-s}$ is dominant, $\sigma(E)$ can be expressed by[2,5,10]

$$\sigma(E) \propto E^{-2/s} \tag{5}$$

This formula is derived from the impact parameter for which orbiting occurs.[24] The condition for the applicability of this

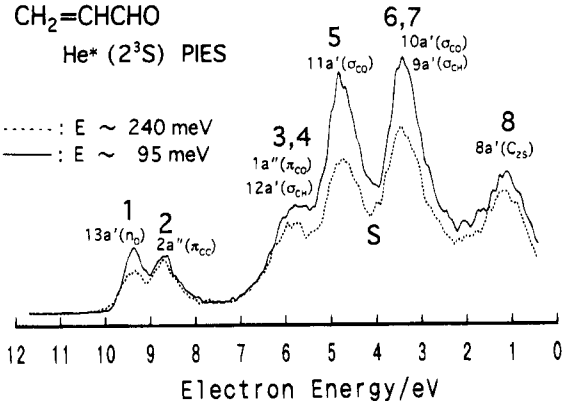


**Figure 6.** Collision-energy-resolved He*($2^3$S) Penning ionization electron spectra of $CH_2CHCHO$ (dashed curve at 240 meV, solid curve at 95 meV).

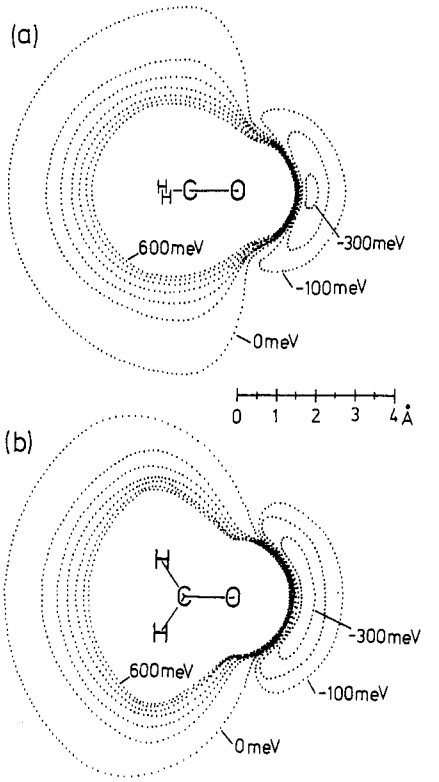


**Figure 7.** Potential energy contour maps for HCHO: (a) contours for out-of-plane including the molecular axis; (b) contours for the molecular plane including nuclear positions of four atoms. Contours were shown with an energy spacing of 100 meV.

equation can be given as ($E < D$), where $D$ is the depth of the attractive potential well. The $s$ parameter determines the steepness of the attractive part of the potential curve and can be obtained from the slope $m$ in the log−log plots of Figures 1−3. The $s$ values obtained are listed in Table 1.

When the condition of $E > D$ is satisfied, the repulsive part of the interaction potential governs $\sigma(E)$. If a small transition probability and the normal incidence for the most effective contributions are assumed, the cross section is then given by the following equation:[2]

$$\sigma(E) \propto \int_{R(0)}^{\infty} \frac{4\pi R^2 W(R) dR}{\sqrt{(2/\mu)[E - V(R)]}} \tag{6}$$

where $W(R)$ is the electronic transition rate at the distance $R$, $V(R)$ is the interaction potential between A* (He*) and M, and $R(0)$ is the shortest distance in the collision trajectory. The

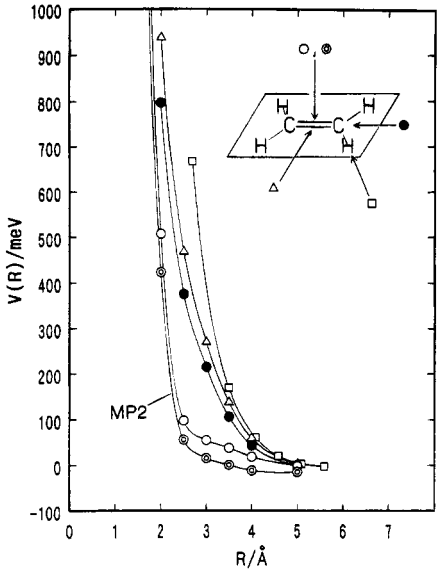


**Figure 8.** Model potential curves $V(R)$ for $C_2H_4$ − He*. In place of He*($1s^12s^1$), Li($1s^22s^1$) is used (see the text). The distance $R$ is measured from the center of mass of the molecule when the He* (Li) atom is located in a plane bisecting the CC bond; otherwise $R$ is measured from the nearest C atom. (○) The potential energy curve (UHF) for out-of-plane access to the center of the CC bond, which is almost completely the same as the curve for out-of-plane access to a carbon atom. (△) The potential energy curve (UHF) for in-plane access to the center of the CC bond. (●) The potential energy curve (UHF) for in-plane access to a carbon atom along the C−C axis. (□) The potential energy curve (UHF) for in-plane access to a hydrogen atom along the C−H axis. (⊙) The potential energy curve(MP2) for the out-of-plane access to the center of the CC bond.

denominator corresponds to the relative velocity at a distance $R$, and its inverse is a factor of the interaction time. Further simplification made by Illenberger and Niehaus[5] yielded the following expression:

$$\sigma(E) \propto E^m \tag{7}$$

where $m$ is expressed by

$$m = (b/d) - (1/2) \tag{8}$$

Parameters $b$ and $d$ determine analytical forms of the interaction potential $V(R)$ and the electronic trnasition probability $W(R)$;

$$V(R) = Ae^{-dR} \tag{9}$$

and

$$W(R) = Be^{-bR} \tag{10}$$

The parameter $d$ is related to the effective steepness of the repulsive potential wall. As discussed in the previous work,[23] the parameter $b$ can be estimated from the asymptotic decay of the target wave function which is directly related to the lowest ionization potential (IP) of the molecule;[35-38]

$$b = 2(2\mathrm{IP})^{1/2} \tag{11}$$

The repulsive potential parameter $d$ can be evaluated from the slope parameter $m$. The obtained $d$ values are listed in Table 1.

**B. HCHO.** As can be seen in Figure 1, all CEDPICS curves for HCHO show negative slopes. This is rather similar to the case of $H_2O$ and $H_2S$, for which all CEDPICS curves for three different ionic states have negative slopes in the log−log plots.[16] This has been ascribed to the strong attractive interaction due to the oxygen or sulfur atom. In the case of $H_2O$ the obtained $s$ values range from 4.4 to 8.3, whereas for $H_2S$ the $s$ values are almost constant around 4 for all three states, due to the charge-induced energy ($s = 4$). In the case of HCHO, the obtained $s$ values in Table 1 range widely from 4.6 to 8.8. The smaller values of 4.6 ($5a_1$) and 5.6 ($2b_2$) can be connected with the charge-induced interaction ($s = 4$) or the permanent-dipole interaction ($s = 6$). However, very large $s$ values over 6 for the ionization from the $1b_1$ or $1b_2$ orbital cannot be ascribed to pure attractive interactions.

Since the most effective geometries for Penning ionization are those of maximum overlap between the target orbital and the inner vacant orbital of the metastable atom (1s orbital of He*),[13,14] the most effective directions causing respective ionic states can be indicated by arrows, as shown in Figure 1. A comparison between the effective directions and the obtained $s$ values indicates that attractive interactions dominate around the oxygen atom. This conjecture is clearly supported by the isopotential energy contour maps in Figure 7. The smaller negative slopes for ionization from $1b_1$ and $1b_2$ orbitals are considered to be due to a repulsive part of the interactions near the hydrogen atoms. The observed negative peak shifts ranging from −0.07 to −0.12 eV also support that attractive interactions are associated with the oxygen atom.

It should be noted that the calculated potential well for HCHO is more extended in the molecular plane (Figure 7b) than in the vertical plane (Figure 7a). This is consistent with the observation that the CEDPICS curve for the in-plane $2b_2$ orbital shows the more attractive characteristics (the larger negative slope in the log−log plot and the larger negative peak shift) than those for the out-of-plane $1b_1$ orbital. Lone-pair electrons in the $sp^2$ hybrids on the O atom are considered to be responsible for the attractive well.

It is interesting to note boundary distances between atoms in HCHO and the Li (He*) atom. At a high collision energy of 600 meV, where the repulsive boundary is nearly converging to the shortest limit, the approximate hard-core radii around constituent atoms can be estimated. Obtained hard-core radii are 1.5 Å for the O atom, 2.0 Å for the C atom, and 1.7 Å for the H atom. Although these radii include the size of the Li (He*) atom, the values are only slightly larger than the van der Waals radii of these atoms,[26] 1.4 Å (O), 1.7 Å (C), and 1.2 Å (H). This indicates that the repulsive boundary around the oxygen atom is extremely shortened due to strong attractive interactions in comparison with the sum of van der Waals radii and the radius of the He* atom.

The attractive potential well and considerably shortened boundary should be the causes of the large enhancement of the $\sigma_{CO}(5a_1)$ band in PIES of HCHO. In the case of the $\sigma_{CO}(5a_1)$ orbital the electron densities are distributed over the attractive well region. On the other hand for the $n_O(2b_2)$ orbital, the electron density is also distributed over the well region, but the existence of the nodal plane reduces the overlap with the incoming He* 1s orbital. Hence, the $n_O(2b_2)$ band is not as enhanced as the $\sigma_{CO}(5a_1)$ band.

**C. $CH_2CH_2$.** The present experiment for $CH_2CH_2$ gave CEDPICS curves of much better qualities than the previous results.[19] As can be seen from Figure 2, the CEDPICS curves show positive slopes except for the $\pi(1b_{2u})$ band. This is interesting because in the case of HCHO, which is an isoelectronic analogue of ethylene ($CH_2CH_2$), the CEDPICS curves entirely decrease with an increase in the collision energy. In Figure 2 the most effective directions causing Penning ionization where electron densities are largely extending outside are shown by the arrows. In the case of $CH_2CH_2$, local interaction

potentials around H atoms are indicated to be repulsive from the observed positive slopes in the CEDPICS. This is confirmed by the model potential curves shown in Figure 8.

Relative hardness of the interaction potential can be compared with the values of the *d* parameter in Table 1. It is noted that a larger *d* value indicates a harder potential wall. The large *d* values of 2.83($1b_{2g}$) and 2.83($1b_{3u}$) are due to interactions at the top of the CH bond, where electron densities are extending outside. The smaller *d* values of 2.57($3a_g$) and 2.57($2b_{1u}$) are due to interactions attacking middle positions of the methylene ($CH_2$) unit, where the corresponding orbitals extend outside. Calculated potential curves in Figure 8 clearly support the relative hardness of the top of the CH bond with respect to the middle of the $CH_2$ unit.

MP2 calculations for $C_2H_4$ showed that potential wells of 15 meV are located at a distance of about 5 Å from the C atom in the CC axis. In view of the difficulty calculating weak interaction energies, this is consistent with the observed small peak shift of −30 meV for the $\pi$ band. The observed negative slope in the CEDPICS for the $\Pi$ state is thus ascribed to attractive potentials such as other unsaturated hydrocarbons, although the experimental range of the collision energy is rather higher than the well depth. If the interactions around the $\pi$ electron regions are attractive, it is of great interest because $\pi$ electrons in unsaturated hydrocarbons have been suggested to behave as Lewis bases to form hydrogen bonds with electron acceptors.[39] However, some comments must be made in this regard. (i) Angular distributions of Penning electrons were found to be highly anisotropic, indicating little effect of attractive potentials.[19] (ii) Potential walls in the perpendicular directions to which $\pi$ electrons are extending outside are found to be very steep (Figure 8). Thus, the negative slopes in the CEDPICS for unsaturated hydrocarbons may possibly arise from the very hard nature of the potential energy surfaces. Even so, calculated anisotropy of the model potentials between A* and M in Figure 8 reveals that the curve for the out-of-plane access to the center of the CC bond, which is almost the same as that for an out-of-plane attack to the C atom, is considerably deformed downward in the tail regions in comparison with smoothly decaying curves for in-plane directions along the CC axis or another in-plane symmetry axis vertical to the CC bond. Therefore, the importance of attractive interactions between $\pi$ electrons and He* $2^3S$ (or Li $2^2S$) atoms must be stressed for unsaturated hydrocarbons.

The approximate sizes of the repulsive boundary around the constituent atoms can be estimated from the calculated potential curves. At the energy of 600 meV, the radii are ca. 2.0 Å for the C atom and 1.7 Å for the H atom. These values agree with those obtained for HCHO.

**D. $CH_2CHCHO$.** In Figure 4 UPS and PIES are compared for *trans*-acrolein ($CH_2CHCHO$) (the trans conformer dominates at room temperature).[40] The assignments in UPS are almost the same as those reported by Kimura et al.[25] except for the first two bands. According to the earlier work,[25] the bands (3, 4) and (6, 7) are assigned to two orbitals, and the band S (IP = ca. 15.5 eV) is assumed to be due to the electron correlation. The small peak (IP = ca. 12.6 eV) indicated by an arrow is due to a small amount of $H_2O$. Contributions of other ionization bands at 14.7 and 18.5 eV due to $H_2O$ are estimated to be much smaller than 4%. In the present study, band 1 is assigned to the $n_O(13a')$ orbital and band 2 to the $\pi_{CC}(2a'')$. The reasons for this assignment are as follows.

(1) Calculated IP values from *ab initio* MO energies for $\pi_{CC}$ orbitals in propene, butene, and butadiene are 0.3−0.5 eV smaller than the observed IP values. If this propensity is transferred to acrolein, the IP value for the $\pi_{CC}$ orbital of acrolein is estimated to be 10.99−11.19 eV, which corresponds to the observed IP value of band 2 (10.92 eV). A similar deduction of the IP value for the $n_O$ orbital on the basis of the calculated and observed IP values for acetaldehyde and propionaldehyde leads to a value of 10.05−10.33 eV, in good agreement with the observed IP value for band 1 (10.10 eV).

(2) In highly resolved UPS,[25] the $n_O$ bands for HCHO and $CH_3CHO$ are very sharp with little vibrational bands, whereas the $\pi$ bands for $CH_2CH_2$, $CH_3CHCH_2$, and $CH_2CHCHCH_2$ have vibrational structures due to the bonding character of the orbitals. In Figure 4 band 1 has no vibrational structure. On the other hand for band 2, vibrational peaks are resolved, and the band envelope is wider than in band 1.

(3) The negative slope in the CEDPICS is steeper for the $n_O$ band (HCHO) than the $\pi_{CC}$ band ($CH_2CH_2$). The observation in the CEDPICS of Figure 3 for $CH_2CHCHO$ supports the present assignment.

The relative intensity in PIES is markedly enhanced for bands 5 and (6, 7). This enhanced intensity can be ascribed to the characteristic electron distributions of the corresponding orbitals of the $\sigma_{CO}$ type (11a′ and 10a′). As in the case of the $5a_1$ orbital of HCHO, electron densities for the $\sigma_{CO}$ orbitals extend outside along the CO double bond having sp hybridization character on the oxygen atom. Since the 9a′ orbital, the other component for the bands (6, 7), has a character around the CO double bond similar to the $1b_2$ orbital of HCHO, which shows a weak band in the PIES of HCHO, then its contribution to the bands (6, 7) of the PIES for acrolein must be very small in comparison with the enhanced contribution of the 10a′ orbital. Therefore, the peak shift and the CEDPICS for the bands (6, 7) discussed below can be ascribed to the 10a′ component.

The CEDPICS curves for $CH_2CHCHO$ in Figure 3 entirely decrease with an increase in the collision energy. The large negative inclinations of −0.4 to −0.3 for bands 1, 5, and (6, 7) are due to attractive interactions around the oxygen atom, as in the case of bands 1 and 3 for HCHO. The smaller inclination for bands (6, 7) can be ascribed to the weak component of the 9a′ orbital, whose electron distributions are dissipated from the oxygen atom. The values of the attractive potential parameter *s* of ca. 5 can be connected with the charge-induced interaction ($s = 4$) or the permanent-dipole interaction ($s = 6$). The strong attractive interactions around the oxygen atom in the C=O group also affect the peak positions of bands 1, 5, and (6, 7). As can be seen in Table 1, the peak energy shifts for bands 1 and 5 are −0.26 and −0.36 eV, respectively. This is consistent with the observation so far made for PIES bands connected with strong attractive interactions. As for the bands (6, 7), if the UPS peak at IP = 16.05 eV is assigned to the 10a′ orbital, the peak energy shift then becomes −0.27 eV, consistent with those for bands 1 and 5.

Relatively small negative inclinations of −0.23 (bands 3, 4: 1a″, 12a′) and −0.18 (band 8: 8a′) in the CEDPICS of Figure 3 can be related with similar values of −0.29 (band 2: $1b_1$) and −0.23 (band 4: $1b_2$) for HCHO. These findings are consistent with the small peak energy shifts of −0.17 eV (bands 3, 4) and 0.02 eV (band 8) for $CH_2CHCHO$ and −0.07 eV (band 2) for HCHO.

Band 2, which can be assigned to the $\pi_{CC}$ orbital as mentioned above, shows no peak energy shift and small negative dependence in the CEDPICS. This indicates that the attractive interaction of $\pi$ electrons with He* is rather weakened. This conjecture is reasonabnle because the presence of the C=O group causes the electron inductive effect as well as the lowering of the $\pi_{CC}$ level (0.41 eV lowered with respect to the case of

$CH_2CH_2$) to result in a weak interaction with the 2s and 2p orbitals of He*; on the basis of the model calculations, the 2s−2p mixing has been found to be responsible for the attractive interactions of target occupied orbitals with He* (Li).

The extra band observed in UPS (IP = ca. 15.5 eV: band S) can be related with the $\pi_{CC}$ orbital from the similar slope of the CEDPICS curves for bands 2 and S in Figure 3. Since band S is not resolved in the PIES, the measurement for the CEDPICS was made at the minimum position (4.1 eV in electron energy). Since the lowest unoccupied orbital of acrolein is an antibonding $\pi$ orbital, band S is suggested to be due to ionization of the occupied bonding $\pi$ orbital associated with a $\pi-\pi^*$ excitation. Such a two-electron process is forbidden without the electron correlation effect. The signal contamination due to a small amount of $H_2O$ (estimated to be less than 4% from UPS) can be neglected also in the PIES.

## VI. Conclusions

The collision energy dependence of partial Penning ionization cross sections reflects that the interaction potential for the investigated molecules with the He*($2^3$S) atom is highly anisotropic depending upon the kind of nearest atom as well as directions with respect to the skeletal structure of the chemical bonding. Intensities of $n_O$ and $\sigma_{CO}$ bands decrease with an increase of the collision energy. This indicates that the interaction potential is attractive if the He*($2^3$S) atom approaches the oxygen atom in the C=O group and is in good agreement with the deep well around the O atom in the calculated potential energy contour maps. The larger negative collision energy dependence for the $n_O$ band than for the $\pi_{CO}$ band shows that the potential well around the O atom is more widely extending along the molecular plane, in agreement with the calculated contour maps for the interaction potentials. Intensities of $\sigma$ bands for $CH_2CH_2$ increase with an increase of the collision energy. This is in contrast with the behavior for the $\sigma$ bands in $CH_2CHCHO$, for which the negative collision energy dependence was observed. In the case of acrolein the attractive interaction around the O atom governs more or less the collisional ionization. On the other hand for ethylene, the local interaction reflects more precisely on the collisional ionization. The repulsive interaction with He* is the strongest at the top of the CH bond. The sideways (horizontal) attacks for the middle of the methylene ($CH_2$) unit undergo relatively soft repulsions. The negative collision energy dependence of the partial ionization cross section for the $\pi_{CC}$ band indicates that attractive interactions are involved for the vertical access of the He*($2^3$S) atom to the $\pi$ electron distributions. The magnitude of the negative peak energy shift is considered as an approximate measure of the depth of the attractive potential well.

Unusually enhanced intensities for the $\sigma_{CO}$ bands in carbonyl compounds are due to large electron densities distributed over the attractive well region with a common phase. Attractive interaction itself does not necessarily lead to the enhancement in PIES.

The assignment of UPS was also reinvestigated. In light of the present PIES results, the ionic-state ordering obtained by the Hartree−Fock *ab initio* calculations was found to disagree with the experiment for acrolein. The existence of the correlation band in the UPS of acrolein suggested by Kimura et al.[25] was given support from the collision energy dependence of the ionization cross section.

**Acknowledgment.** This work has been supported by a Grant in Aid (No. 03403004) for Scientific Research from the Japanese Ministry of Education, Science, and Culture.

## References and Notes

(1) Penning, F. M. *Naturwissenshaften* **1927**, *15*, 818.
(2) Niehaus, A. *Adv. Chem. Phys.* **1981**, *45*, 399.
(3) Yencha, A. J. *Electron Spectroscopy: Theory, Technique, and Applications*; Brundle, C. R., Baker, A. D., Eds.; Academic: New York, 1984, Vol. 5.
(4) Siska, P. E. *Rev. Mod. Phys.* **1993**, *65*, 337.
(5) Illenberger, E.; Niehaus, A. *Z. Phys. B* **1975**, *20*, 33.
(6) Parr, T. P.; Parr, D. M.; Martin, R. M. *J. Chem. Phys.* **1982**, *76*, 316.
(7) Pesnelle, A.; Watel, G.; Manus, C. *J. Chem. Phys.* **1975**, *62*, 3590.
(8) Woodard, M. R.; Sharp, R. C.; Seely, M.; Muschlitz, E. E., Jr. *J. Chem. Phys.* **1978**, *69*, 2978.
(9) Appolloni, L.; Brunetti, B.; Hermanussen, J.; Vecchiocativi, F.; Volpi, G. G. *J. Chem. Phys.* **1978**, *69*, 2978.
(10) Allison, W.; Muschlitz, E. E., Jr. *J. Electron Spectrosc. Relat. Phenom.* **1981**, *23*, 339.
(11) Riola, J. P.; Howard, J. S.; Rundel, R. D.; Stebbings, R. F. *J. Phys. B* **1974**, *7*, 376.
(12) Lindinger, W.; Schmeltekopf, A. L.; Fehsenfelt, F. C. *J. Chem. Phys.* **1974**, *61*, 2890.
(13) Ohno, K.; Mutoh, H.; Harada, Y. *J. Am. Chem. Soc.* **1983**, *105*, 4555.
(14) Ohno, K.; Harada, Y. In *Theoretical Models of Chemical Bonding*; Maksić, Z. B., Ed.; Springer-Verlag: Berlin−Heidelberg, 1991; Part 3, pp 199−234.
(15) Čermák, V. *J. Chem. Phys.* **1966**, *44*, 3781.
(16) Mitsuke, K.; Takami, T.; Ohno, K. *J. Chem. Phys.* **1989**, *91*, 1618.
(17) Ohno, K.; Takami, T.; Mitsuke, K.; Ishida, T. *J. Chem. Phys.* **1991**, *94*, 2675.
(18) Takami, T.; Mitsuke, K.; Ohno, K. *J. Chem. Phys.* **1991**, *95*, 918.
(19) Takami, T.; Ohno, K. *J. Chem. Phys.* **1992**, *96*, 6523.
(20) Pasinszki, T.; Yamakado, H.; Ohno, K. *J. Phys. Chem.* **1993**, *97*, 12718.
(21) Dunlavy, D. C.; Martin, D. W.; Siska, P. E. *J. Chem. Phys.* **1990**, *93*, 5347.
(22) Longley, E. J.; Dunlavy, D. C.; Falcetta, M. F.; Bevsek, H. M.; Siska, P. E. *J. Phys. Chem.* **1993**, *97*, 2097.
(23) Mitsuke, K.; Kusafuka, K.; Ohno, K. *J. Phys. Chem.* **1989**, *93*, 3062.
(24) Gardner, J. L.; Samson, J. A. R. *J. Electron Spectrosc. Relat. Phenom.* **1976**, *8*, 469.
(25) Kimura, K.; Katsumata, S.; Achiba, Y.; Yamazaki, T.; Iwata, S. *Handbook of He I Photoelectron Spectra of Fundamental Organic Molecules*; Japan Scientific: Tokyo, 1981.
(26) Hehre, W. J.; Radom, L.; Schleyer, P. v. R.; Pople, J. A. *Ab Initio Molecular Orbital Theory*; John Wiley & Sons: New York, 1986.
(27) Rothe, E. W.; Neynaber, R. H.; Trujillo, S. M. *J. Chem. Phys.* **1965**, *42*, 3310.
(28) Hotop, H. *Radiat. Res.* **1974**, *59*, 379.
(29) Haberland, H.; Lee, Y. T.; Siska, P. E. *Adv. Chem. Phys.* **1981**, *45*, 487.
(30) Frisch, M. J.; Trucks, G. W.; Head-Gordon, M.; Gill, P. M.; Wong, M. W.; Foresman, J. B.; Johnson, B. G.; Schlegel, H. B.; Robb, M. A.; Replogle, E. S.; Gomperts, R.; Andres, J. L.; Raghavachari, K.; Binkley, J. S.; Gonzalez, C.; Martin, R. L.; Fox, D. J.; Defrees, D. J.; Baker, J.; Stewart, J. J. P.; Pople, J. A. *Gaussian 92*; Gaussian, Inc.: Pittsburgh, PA, 1992.
(31) Ohno, K.; Sunada, S. *Proc. Indian Acad. Sci. (Chem. Sci.)* **1994**, *106*, 327.
(32) Ohno, K.; Takano, S.; Mase, K. *J. Phys. Chem.* **1986**, *90*, 2015.
(33) Pauling, L. *The Nature of the Chemical Bond*; Cornell University: Ithaca, NY, 1960.
(34) Ohno, K.; Matsumoto, S.; Harada, Y. *J. Chem. Phys.* **1984**, *81*, 4447.
(35) Handy, N. C.; Marron, M. T.; Silverstone, H. J. *Phys. Rev.* **1969**, *180*, 45.
(36) Ahlrichs, R. *Chem. Phys. Lett.* **1973**, *18*, 521.
(37) Morrell, M. M.; Parr, R. G.; Levy, M. *J. Chem. Phys.* **1975**, *62*, 549.
(38) Katriel, J.; Davidson, E. R. *Proc. Natl. Acad. Sci. U.S.A.* **1980**, *77*, 4403.
(39) Rodham, D. A.; Suzuki, S.; Suenram, R. D.; Lovas, F. J.; Dasgupta, S.; Goddard, W. A., III; Blake, G. A. *Nature* **1993**, *362*, 735 and references cited therein.
(40) Wagner, R.; Fine, J.; Simmons, J. W.; Goldstein, J. H. *J. Chem. Phys.* **1957**, *26*, 634.

JP9503425